31st Annual International Conference of the IEEE EMBS
Minneapolis, Minnesota, USA, September 2-6, 2009

Perturbation Analysis of the Effects of B_1^+ Errors on Parallel Excitation in MRI

Chao Ma, Dan Xu, Kevin F. King and Zhi-Pei Liang

***Abstract*— Design of RF pulses for parallel excitation using phased array transmit coils in MRI requires the B_1^+ maps that are estimated from B_1^+ mapping experiments. This paper characterizes the effects of B_1^+ mapping errors on the resulting excitation pattern using a small perturbation analysis based on linearization of the Bloch equation. The accuracy of the proposed perturbation analysis is validated by Bloch equation simulations based on experimental B_1^+ maps. The perturbation analysis builds a transparent connection between the B_1^+ mapping errors and the resulting excitation errors, and can be used to study the robustness of the designed RF pulses to B_1^+ mapping errors. The proposed method may also supply useful metrics for designing RF pulses that are robust to B_1^+ mapping errors.**

I. INTRODUCTION

In MR imaging, radio frequency (RF) pulses are used to flip the bulk magnetization. Frequency-selective RF pulses can be made spatially selective when they are applied in the presence of a gradient field. The most commonly used selective RF pulses are 1D slice-selective RF pulses. Multidimensional spatially-selective RF pulses (or simply multidimensional RF pulses) have many applications such as reduced field-of-view (FOV) imaging [1] and B_1^+ inhomogeneity correction in high field MR imaging [2]. However, the multidimensional RF pulses are often very long (20-100 ms) [3], which significantly limit their practical utility. Recently parallel excitation [4], [5] has emerged as a promising approach to shorten multidimensional RF pulses by driving phased array transmit coils simultaneously.

Most RF pulse design methods [4], [5], [6], [7] in parallel excitation require knowledge of sensitivities of phased array transmit coils (or simply B_1^+ maps), whose accuracies are, in practice, often limited by signal-to-noise ratio (SNR) and resolution of B_1^+ mapping data and modeling error of B_1^+ mapping methods. It is, therefore, important to characterize the effects of B_1^+ mapping errors on the resulting excitation pattern. Suppose there are L phased array transmit coils. The question addressed in this paper is: given a set of RF pulses $\{b_{1,l}(\vec{r})\}_{l=1}^L$ designed based on estimated B_1^+ maps $\{S_l(\vec{r})\}_{l=1}^L$, what is the excitation error if the actual B_1^+ maps are $\{S_l(\vec{r})+\Delta S_l(\vec{r})\}_{l=1}^L$? More specifically, let $\vec{M}_d(\vec{r},t)$ and $\vec{M}_a(\vec{r},t)$ be the solution of the Bloch equation (ignoring the relaxation):

$$\begin{bmatrix}\dot{M}_x(\vec{r},t)\\ \dot{M}_y(\vec{r},t)\\ \dot{M}_z(\vec{r},t)\end{bmatrix} = \gamma \begin{bmatrix}0 & \vec{G}(t)\cdot\vec{r} & -B_{1,y}(\vec{r},t)\\ -\vec{G}(t)\cdot\vec{r} & 0 & B_{1,x}(\vec{r},t)\\ B_{1,y}(\vec{r},t) & -B_{1,x}(\vec{r},t) & 0\end{bmatrix} \times \begin{bmatrix}M_x(\vec{r},t)\\ M_y(\vec{r},t)\\ M_z(\vec{r},t)\end{bmatrix}, \quad (1)$$

for a given gradient field $\vec{G}(t)\cdot\vec{r}$ and RF fields $B_1(\vec{r},t) = \sum_{l=1}^L b_{1,l}(t)S_l(\vec{r})$ (the designed RF field) and $B_1(\vec{r},t) = \sum_{l=1}^L b_{1,l}(t)[S_l(\vec{r}) + \Delta S_l(\vec{r})]$ (the actual RF field) respectively, what is the difference between $\vec{M}_d(\vec{r},T)$ (the designed excitation pattern) and $\vec{M}_a(\vec{r},T)$ (the actual excitation pattern), where T is the pulse length.

The problem is trivial if the Bloch equation has a closed-form solution. However, this is not the case for a general $B_1(\vec{r},t)$. We could solve the Bloch equation numerically for a given pulse, but such an approach doesn't provide useful insights for the general case. In this paper, we use a perturbation analysis developed by Grissom [8] for RF pulse design to address our problem.

The remaining of this paper is organized as follows. First, a small perturbation analysis of the excitation error $\Delta\vec{M}(\vec{r},T) = \vec{M}_a(\vec{r},t) - \vec{M}_d(\vec{r},t)$ is presented. The accuracy of the perturbation analysis is then discussed based on numerical solution of the Bloch equation.

II. PERTURBATION ANALYSIS

For the convenience of analysis, we make use of the spin-domain Bloch equation [9]. More specifically, the Cayley-Klein parameters (or simply spinor parameters) α and β of the designed excitation pattern are calculated by solving the following differential equations:

$$\begin{bmatrix}\dot{\beta}\\ \dot{\alpha}^*\end{bmatrix} = \frac{i\gamma}{2}\begin{bmatrix}\vec{G}\cdot\vec{r}, & B_1^*\\ B_1, & -\vec{G}\cdot\vec{r}\end{bmatrix}\begin{bmatrix}\beta\\ \alpha^*\end{bmatrix}, \quad (2)$$

where $B_1(\vec{r},t) = \sum_{l=1}^L b_{1,l}(t)S_l(\vec{r})$, "*" denotes conjugate transpose, and the depedence of variables on spatial location $\vec{r}$ and time t are dropped for simplicity of the expression.

Given the initial condition of the magnetization $[M_{xy}(0), M_{xy}^*(0), M_z(0)]^{\mathrm{T}}$ ("T" denotes transpose), at the end of the RF pulse, the designed magnetization is calculated by:

$$\begin{bmatrix}M_{xy}(T)\\ M_{xy}^*(T)\\ M_z(T)\end{bmatrix} = \begin{bmatrix}(\alpha^*)^2 & -(\beta^*)^2 & -2\alpha^*\beta^*\\ -\beta^2 & \alpha^2 & -2\alpha\beta\\ \alpha^*\beta & \alpha\beta^* & \alpha\alpha^* - \beta\beta^*\end{bmatrix}\begin{bmatrix}M_{xy}(0)\\ M_{xy}^*(0)\\ M_z(0)\end{bmatrix}, \quad (3)$$

This work was supported by the grant NSF-CBET-07-30623.

C. Ma and Z.-P. Liang are with the Department of Electrical and Computer Engineering, University of Illinois at Urbana-Champaign, Urbana, IL 61801. chaoma2, z-liang@illinois.edu

D. Xu and K.F. King are with the Applied Science Laboratory, GE Healthcare, Waukesha, WI 53188.

where $M_{xy} = M_x + iM_y$ is the transverse component of the magnetization, and α and β are evaluated at time T.

Denote the actual RF field as $B_1(\vec{r},t) + \Delta B_1(\vec{r},t)$, where $\Delta B_1(\vec{r},t) = \sum_{l=1}^{L} b_{1,l}(t)\Delta S_l(\vec{r})$ is considered as a perturbation term on the RF field $B_1(\vec{r},t)$. Then the spinor parameters of the actual excitation pattern are calculated by solving the following differential equations:

$$\begin{bmatrix} \dot{\beta}+\dot{\tilde{\beta}} \\ \dot{\alpha}^*+\dot{\tilde{\alpha}}^* \end{bmatrix} = \frac{i\gamma}{2}\begin{bmatrix} \vec{G}\cdot\vec{r}, & B_1^*+\Delta B_1^* \\ B_1+\Delta B_1, & -\vec{G}\cdot\vec{r} \end{bmatrix}\begin{bmatrix} \beta+\tilde{\beta} \\ \alpha^*+\tilde{\alpha}^* \end{bmatrix}, \tag{4}$$

where $\tilde{\alpha}$ and $\tilde{\beta}$ are the corresponding perturbations on the spinor parameters.

Subtracting Eq. (2) from Eq. (4), we obtain the following differential equations to calculate the perturbations of the spinor parameters:

$$\begin{cases} \dot{\tilde{\beta}} = \frac{i\gamma}{2}\big(\vec{G}\cdot\vec{r}\tilde{\beta} + B_1^*\tilde{\alpha}^* + \Delta B_1^*\alpha^* + \Delta B_1^*\tilde{\alpha}^*\big), \\ \dot{\tilde{\alpha}}^* = \frac{i\gamma}{2}\big(B_1\tilde{\beta} + \Delta B_1\beta + \Delta B_1\tilde{\beta} - \vec{G}\cdot\vec{r}\tilde{\alpha}^*\big). \end{cases} \tag{5}$$

However, Eq. (5) in general does not have a closed-form solution, and therefore supplies few useful insights for analysis. To get an approximate closed-form solution of the perturbations of the spinor parameters, we follow a derivation in [8], where the same solution is used for designing RF pulses. Suppose the difference between the actual RF field and the designed RF field, *i.e.* $\Delta B_1(\vec{r},t)$, is relatively small compared with the designed RF field $B_1(\vec{r},t)$, we ignore all the second order terms: $\Delta B_1^*\tilde{\alpha}^*$ and $\Delta B_1\tilde{\beta}$. We further assume $B_1^*\tilde{\alpha}^*$ and $B_1\tilde{\beta}$ are relatively small compared with other terms, and therefore ignore these two terms in Eq. (5), which yields the following decoupled differential equations:

$$\begin{cases} \dot{\tilde{\beta}} = \frac{i\gamma}{2}\big(\vec{G}\cdot\vec{r}\tilde{\beta} + \Delta B_1^*\alpha^*\big), \\ \dot{\tilde{\alpha}}^* = \frac{i\gamma}{2}\big(\Delta B_1\beta - \vec{G}\cdot\vec{r}\tilde{\alpha}^*\big). \end{cases} \tag{6}$$

Note that the initial conditions of Eq. (6) are: $\tilde{\beta}(\vec{r},0) = 0, \tilde{\alpha}(\vec{r},0) = 0$, because no RF field is applied at $t = 0$. We finally obtain a closed-form solution of $\tilde{\beta}$ and $\tilde{\alpha}$. At the end of RF pulse, the closed-form solution is given by:

$$\begin{cases} \tilde{\beta}(\vec{r},T) \approx \sum_{l=1}^{L}\Delta S_l^*(\vec{r})c_l(\vec{r},T), \\ \tilde{\alpha}^*(\vec{r},T) \approx \sum_{l=1}^{L}\Delta S_l(\vec{r})d_l(\vec{r},T), \end{cases} \tag{7}$$

where denoting $\vec{k}(t) = -\gamma\int_t^T \vec{G}(s)ds$ known as the excitation k-space trajectory, $c_l(\vec{r},T)$ and $d_l(\vec{r},T)$ are defined as:

$$\begin{cases} c_l(\vec{r},T) \triangleq \frac{i\gamma}{2}\int_0^T b_{1,l}^*(t)\alpha^*(\vec{r},t)e^{-\frac{i}{2}\vec{r}\cdot\vec{k}(t)}dt, \\ d_l(\vec{r},T) \triangleq \frac{i\gamma}{2}\int_0^T b_{1,l}(t)\beta(\vec{r},t)e^{\frac{i}{2}\vec{r}\cdot\vec{k}(t)}dt. \end{cases} \tag{8}$$

Once the perturbations of the spinors parameters are calculated, we can then calculate the perturbation of the excitation pattern based on Eq. (3). As a specific case, for the excitation RF pulse, where the initial state of $\vec{M}$ is normalized to be $[0,0,1]^{\mathrm{T}}$, the perturbation of the transverse component of the excitation pattern is given by:

$$\begin{aligned} \Delta M_{xy}(\vec{r},T) \approx -2\sum_{l=1}^{L}\big[&\alpha^*(\vec{r},T)c_l^*(\vec{r},T) \\ &+\beta^*(\vec{r},T)d_l(\vec{r},T)\big]\Delta S_l(\vec{r}), \end{aligned} \tag{9}$$

where second order perturbation terms are dropped.

In summary, in order to calculate the perturbation of the excitation pattern, we need to know the difference between the actual and the estimated B_1^+ maps, *i.e.* $\Delta S_l(\vec{r})$, and the unperturbed spinor parameters $\alpha(\vec{r},t)$ and $\beta(\vec{r},t)$, which can be calculated by solving the Bloch equation numerically with a given gradient field $\vec{G}(t)\cdot\vec{r}$, designed RF waveforms $b_{1,l}(t)$ and estimated B_1^+ maps $S_l(\vec{r})$.

III. VALIDATION

The accuracy of the perturbation analysis replies on how well the two assumptions we make in the derivation of Eqs. (7) and (8) are satisfied. On the one hand, the accuracy of the perturbation analysis depends on the accuracy of the estimated B_1^+ maps since we ignore the second order terms $\Delta B_1^*\tilde{\alpha}^*$ and $\Delta B_1\tilde{\beta}$ in Eq. (5) by assuming the perturbation of the RF field $\Delta B_1(\vec{r},t)$ caused by B_1^+ mapping errors is relatively small with respect to the RF field $B_1(\vec{r},t)$. On the other hand, with a fixed gradient field and fixed pulsed length, the accuracy of the perturbation analysis will also depends on the flip angle since the contribution of the ignored terms $B_1^*\tilde{\alpha}^*$ and $B_1\tilde{\beta}$ in Eq. (5) will increase as the flip angle increases. In the remaining of this section, we discuss the accuracy of the perturbation analysis with respect to the accuracy of the estimated B_1^+ maps and the flip angle by Bloch equation simulations based on experimental B_1^+ maps.

The estimated B_1^+ maps were collected at a 3T GE scanner with a two-channel parallel transmit coil. The gradient waveform was determined by a 10-turn spiral-in excitation k-space trajectory. The RF pulses were designed to achieve a 2D reduced FOV excitation pattern using a linear class large-flip-angle design method [6]. Since the validation of the perturbation analysis doesn't rely on specific distributions of B_1^+ mapping errors, for the convenience of result comparison, we assumed that the actual B_1^+ maps were the estimated B_1^+ maps plus i.i.d Gaussian noise with a standard deviation σ. To quantitatively characterize the accuracy of the estimated B_1^+ map, we define the average SNR of the estimated B_1^+ map as the energy of the estimation error divided by the energy of the actual B_1^+ map.

Solving the Bloch equation with the designed RF pulses and the estimated B_1^+ maps, we obtained the designed excitation pattern. Solving the Bloch equation with the designed RF pulses and the actual B_1^+ maps, we obtained the actual excitation pattern and the corresponding excitation error. Repeating Bloch equation simulations, we calculated the standard deviation of the excitation error. We were particularly interested in the standard deviation of the transverse component of the excitation error, because the transverse component would directly contribute to receiving signals. We treated the standard deviation of the excitation error calculated by repeating Bloch equation simulations as the gold standard, and compared it with the standard deviation calculated by the perturbation analysis, which is, based on

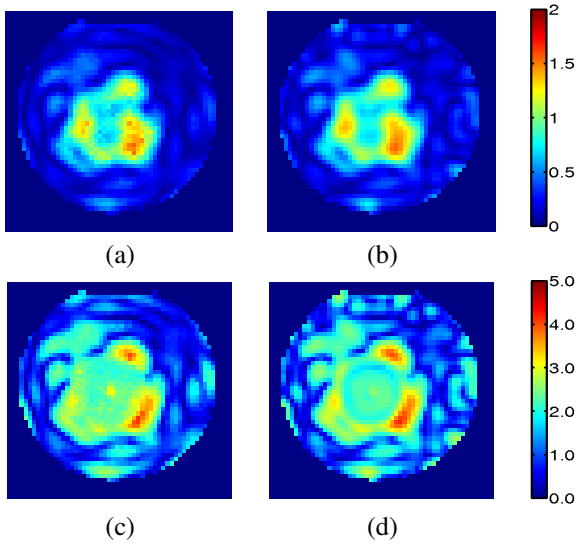

Fig. 1. The true standard deviation of the excitation error vs. the one estimated by the perturbation analysis. The average SNR of the estimated B_1^+ maps is 20 dB. (a) and (c): The true standard deviations with 30° and 90° flip angle respectively. (b) and (d): The standard deviations estimated by the perturbation analysis (Eq. (10)) with 30° and 90° flip angle respectively.

Eq. (9), given by:

$$\sigma_{\Delta M_{xy}}(\vec{r},T) \approx 2\sigma\Big[\sum_{l=1}^{L}|\alpha^*(\vec{r},T)c_l^*(\vec{r},T) + \beta^*(\vec{r},T)d_l(\vec{r},T)|^2\Big]^{1/2}. \quad (10)$$

Figure 1 shows the true standard deviations of the excitation errors (or simply the true standard deviations) (Fig. 1 (a) and (c)) and the ones estimated by the perturbation analysis (Fig. 1 (b) and (d)), *i.e.* by Eq. (10), with 30° and 90° flip angle respectively. The magnitude and, more importantly, the pattern of the standard deviation estimated by the perturbation analysis have a very good match with the true ones for both 30° and 90° flip angle. To further quantitatively study the accuracy of the perturbation analysis with respect to the flip angle, we calculate the root-mean-square error (RMS error) of the standard deviation estimated by the perturbation analysis. In Fig. 2 (a), we plot the RMS error as a function of flip angle. The RMS error increases as the flip angle increases because the contribution of the ignored terms $B_1^*\tilde{\alpha}^*$ and $B_1\tilde{\beta}$ in Eq. (5) increases with increasing flip angles. However, the RMS error is below 10% for flip angles from 10° to 90°. The above results indicate that the perturbation analysis is applicable to both small-flip-angle and large-flip-angle RF pulses.

Figure 2 (b) shows the plot of the RMS error of the standard deviation estimated by the perturbation analysis as a function of average SNR of the estimated B_1^+ maps. The RMS error is below 10% for a wide range of average SNR of the estimated B_1^+ maps (from 30dB to 5dB). As the average SNR further decreases, the RMS error quickly increases. That is because the perturbation of the RF field caused by the B_1^+ mapping errors cannot be assumed to be small, and the perturbation analysis becomes not validate in these cases. This result demonstrates that the perturbation analysis is applicable to a large range of average SNR of the estimated B_1^+ maps.

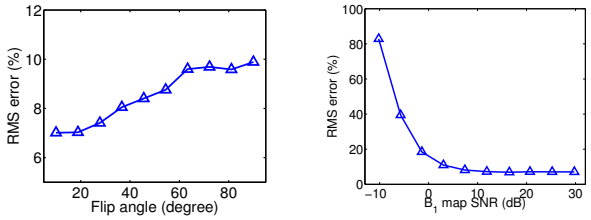

Fig. 2. (a): The RMS error of the standard deviation estimated by the perturbation analysis vs. the flip angle, where the average SNR of the estimated B_1^+ maps is 20 dB. (b): The RMS error of the standard deviation estimated by the perturbation analysis vs. the average SNR of the estimated B_1^+ maps, where the flip angle is 60°

IV. CONCLUSIONS

In this paper, we present a perturbation analysis of the effects of B_1^+ mapping errors on the resulting excitation pattern based on linearization of the Bloch equation. Experimental B_1^+ maps based Bloch equation simulations demonstrate that the perturbation analysis is validate for both small-flip-angle and large-flip-angle RF pulses, and for a wide range of average SNR of the estimated B_1^+ maps.

The perturbation analysis builds a transparent connection between the B_1^+ mapping errors and the resulting excitation error, and can be used to study the robustness of the designed RF pulses to B_1^+ mapping errors with different RF design parameters, for instance flip angle, reduction factor, and excitation k-space trajectory. The perturbation analysis may also supply useful metrics for designing RF pulses that are robust to B_1^+ mapping errors.

REFERENCES

[1] S. Rieseberg, J. Frahm and J. Finsterbusch, Two-dimensional spatially-selective RF excitation pulses in echo-planar imaging, *Magn Reson Med*, vol. 47, 2002, pp 1186-1193.

[2] S. Saekho, C.Y. Yip, D.C. Noll, F.E. Boada, and V.A. Stenger, Fast-k_z three-dimensional tailored radiofrequency pulse for reduced B1 inhomogeneity, *Magn Reson Med*, vol. 55, 2006, pp 719-724.

[3] V. A. Stenger, F.E. Boada, and D.C. Noll, Multishot 3D Slice-Select Tailored RF Pulses for MRI, *Magn Reson Med*, vol. 48, 2002, pp 157-165.

[4] U. Katscher, P. Bornert, C. Leussler, and J.S. van den Brink, Transmit SENSE, *Magn Reson Med*, vol. 49, 2003, pp 144-150.

[5] Y. Zhu, Parallel excitation with an array of transmit coils, *Magn Reson Med*, vol. 51, 2004, pp 775-784.

[6] D. Xu, K.F. King, Y. Zhu, G.C. McKinnon, and Z.P. Liang, A non-iterative method to design large-tip-angle multidimensional spatially-selective radio frequency pulses for parallel transmission, *Magn Reson Med*, vol. 58, 2007, pp 326 - 334.

[7] D. Xu, K.F. King, Y. Zhu, G.C. McKinnon, and Z.P. Liang, Designing multichannel, multidimensional, arbitrary flip angle RF pulses using an optimal control approach, *Magn Reson Med*, vol. 59, 2008, pp 547-560.

[8] W. Grissom, RF pulse design for parallel excitation in MRI, *PhD thesis, University of Michigan*, 2008.

[9] J. Pauly, D. Nishimura and A. Macovski, A linear class of large-tip-angle selective excitation pulses, *J. Magn Reson*, vol. 82, 1989, pp 571-587.